EXPERIMENTAL EVIDENCE FOR STATISTICAL SCALING AND INTERMITTENCY IN SEDIMENT TRANSPORT RATES

By

Arvind Singh

Kurt Fienberg

Douglas J. Jerolmack

Jeffrey Marr

and

Efi Foufoula-Georgiou

IMA Preprint Series # 2237

(February 2009)

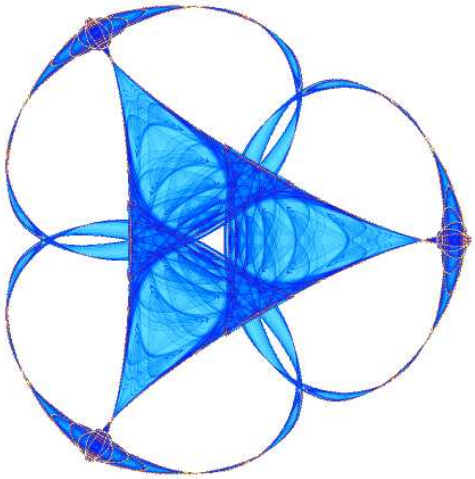

INSTITUTE FOR MATHEMATICS AND ITS APPLICATIONS

UNIVERSITY OF MINNESOTA

400 Lind Hall
207 Church Street S.E.
Minneapolis, Minnesota 55455–0436

Phone: 612-624-6066 Fax: 612-626-7370
URL: http://www.ima.umn.edu

Experimental evidence for statistical scaling and intermittency in sediment transport rates

Arvind Singh[1], Kurt Fienberg[1], Douglas J. Jerolmack[2], Jeffrey Marr[1],

and Efi Foufoula-Georgiou[1]

[1]St. Anthony Falls Laboratory and National Center for Earth-surface Dynamics,
Dept. of Civil Engineering,
University of Minnesota
2 Third Ave. SE, Minneapolis MN, USA.

[2] Department of Earth and Environmental Science,
University of Pennsylvania
Hayden Hall, 240 S. 33rd St., Philadelphia, PA , USA.

Journal of Geophysical Research, Earth Surface

Submitted December 2007

Revised August 2008

Re-revised November 2008

Abstract

Understanding bed load transport fluctuations in rivers is crucial for development of a transport theory, and for choosing a sampling interval for "mean" transport rates. Field-scale studies lack sufficient resolution to statistically characterize these fluctuations, while laboratory experiments are limited in scale and hence cannot be directly compared to field cases. Here we use a natural-scale laboratory channel to examine bed load transport fluctuations in a heterogeneous gravel substrate under normal flow conditions. The novelty of our approach is the application of a geometrical/statistical formalism (called the multifractal formalism), which allows characterization of the "roughness" of the series (depicting the average strength of local abrupt fluctuations in the signal) and the "intermittency" (depicting the temporal heterogeneity of fluctuations of different strength). We document a rougher and more intermittent behavior in bedload sediment transport series at low discharge conditions, transitioning to a smoother and less intermittent behavior at high discharge conditions. We derive an expression for the dependence of the probability distribution of bedload sediment transport rates on sampling interval. Our findings are consistent with field observations demonstrating that mean bedload sediment transport rate decreases with sampling time at low transport conditions and increases with sampling time at high transport conditions. Simultaneous measurement of bed elevation suggests that the statistics of sediment transport fluctuations are related to the statistics of bed topography.

Keywords: scaling, fractal, turbulence, bed form, dunes, ripples

1. Introduction

Measurements of bed load transport rates are fundamental to estimating material transport in a river, yet even defining a representative time period over which to sample is difficult due to the inherent variability and stochastic character of sediment transport. This variability is present over a wide range of scales, from the movement of individual grains [*Iseya and Ikeda,* 1987*; Drake et al.,* 1988; *Nikora et al.,* 2002; *Schmeeckle and Nelson,* 2003; *Sumer et al.*, 2003; *Ancey et al.,* 2008] up to the propagation of dunes and bars [*Kuhnle and Southard,* 1988; *Gomez et al.,* 1989; *Cudden and Hoey,* 2003; *Jerolmack and Mohrig,* 2005], even under steady flow conditions. Computed statistics of instantaneous bed load transport rates (flux) have shown that probability distributions are often skewed toward larger values [e.g., *Gomez et al.,* 1989], implying a high likelihood of extreme fluctuations, the prediction of which is essential for protecting hydraulic structures and assessing the stability of riverine habitat [*Yarnell et al.,* 2006]. It has also been observed that the mean sediment flux depends on the time interval (sampling time) over which the mean is computed, and previous work has suggested that this time dependence is the result of large, infrequent transport events [see *Bunte and Abt*, 2005*,* and references therein].

An analogous time-dependence that has been more thoroughly studied is that of the sedimentary record, where apparent deposition rate (measured from two dated surfaces) diminishes rapidly with measurement duration in virtually all depositional environments [*Sadler*, 1981; 1999]. Models show that this scale dependence is a direct result of the statistics of transport fluctuations [e.g., *Jerolmack and Sadler*, 2007]. In the case of geologic rates the data have been assumed to obey simple scaling over a wide range of time scales, i.e. the statistical moments can be fitted as power-law functions of scale, with the exponents linear in moment order. This power-law relationship provides a value for the Hurst exponent, H, which may be used to compare rates at one scale to rates at a different scale via a simple statistical transformation (see also discussion that follows). However, many geophysical processes exhibit

multiscaling (or multifractal behavior), which implies that a range of exponents (and not a single exponent) is required to describe the changes in the probability density function (pdf) with scale. Examples include rainfall intensities [e.g., *Lovejoy and Schertzer*, 1985; *Venugopal et al.,* 2006b], cloud structures [e.g., *Lovejoy et al.,* 1993; *Arneodo et al.*, 1999a], river flows [e.g., *Gupta and Waymire*, 1996], river network branching topologies [e.g., *Rinaldo et al.*, 1993; *Marani et al.*, 1994; *Lashermes and Foufoula-Georgiou*, 2007], braided river systems [e.g., *Foufoula-Georgiou and Sapozhnikov,* 1998], and valley morphology [e.g., *Gangodagamage et al.*, 2007]. This rich multiscale statistical structure includes extreme but rare fluctuations ("bursts") that occur inhomogeneously over time, giving rise to the so-called "intermittency" and leading to a nontrivial scaling of the statistical moments. A prime example of this is the velocity fluctuations in fully developed isotropic turbulence [e.g., *Parisi and Frisch*, 1985; *Frisch*, 1995; *Arneodo et al.*, 1999b].

To the best of our knowledge, bedload sediment transport series have not been analyzed before from the perspective of quantifying how the statistical moments of the series change with scale. In an early study *Gomez et al.*, [1989] acknowledged that the probability distribution of sediment transport rates depends on sampling time (scale) and extended the Einstein and Hamamori distributions to a scale-dependent form, without however attempting any scale-renormalization. Knowledge of the variability inherent in bed load transport rates at all scales is essential for quantifying material flux, for designing appropriate measurement programs, and for comparison among different data sets and model predictions at different temporal and spatial scales. Also, quantifying the statistical structure of these fluctuations across scales may yield insight into the fundamental physics of sediment transport and provide a set of diagnostics against which to rigorously test competing theories and bed load transport models [see also *Ancey et al.,* 2006; 2008].

One would expect that the statistics of bed load sediment transport would relate in some way to the statistics of the fluctuations in bed elevation. Although river bed elevations have been

116 analyzed much more than sediment fluxes and have been found to exhibit fluctuations across a
117 wide range of scales, in both sandy [e.g., *Nikora et al.,* 1997; *Nikora and Hicks*, 1997; *Jerolmack*
118 *and Mohrig*, 2005] and gravelly [*Dinehart*, 1992; *Nikora and Walsh*, 2004; *Aberle and Nikora*,
119 2006] systems, the link between bed topography and sediment flux remains largely unexplored
120 due to the difficulty in simultaneous data acquisition. Establishing a relationship between the
121 statistics of bed elevations and sediment transport rates is important for effective modeling of
122 river bed morphodynamics and also for understanding the physics of sediment transport. More
123 practically, since bed elevation data are far easier to collect than sediment flux measurements, an
124 understanding of how the statistics of the one variable relate to those of the other, at least over a
125 range of temporal scales, could greatly facilitate estimating sediment transport rate in the field.
126 To address these issues we present here an analysis of data from a unique experimental
127 laboratory setup capable of mimicking transport conditions in the field (see section 3). High
128 resolution, long duration time series of sediment transport rates and bed elevation were
129 simultaneously collected in a suite of experiments with a heterogeneous gravel bed. We use the
130 multifractal formalism, originally developed for fluid turbulence [*Parisi and Frisch*, 1985;
131 *Frisch*, 1995; *Muzy et al.*, 1994], to quantify the "roughness" (the average strength of local
132 burstiness in the signal) and the "intermittency" (the temporal variability or heterogeneity of
133 bursts of different strengths) and relate those geometrical quantities to the statistics of sediment
134 flux and bed topography over a range of time scales. (Note that throughout the paper the term
135 "roughness", as defined mathematically via the strength of local singularities, refers to the signal
136 roughness being that sediment transport rates or bed elevation fluctuations and it is not to be
137 confused with other uses of the term roughness such as bed roughness or hydraulic roughness.)
138 We substantiate the findings of *Bunte and Abt* [2005] that mean sediment transport rate
139 diminishes with increasing sampling time at low bed stress (slightly above critical) but does the
140 opposite for high transport conditions, and we relate this reversal in trend to the influence of
141 large-scale bed forms. Our analysis also allows characterization of the sampling time dependence

142 of all of the statistical moments, allowing thus the prediction of extremes at small scales from the
143 statistics at larger scales.
144
145 **2. Experimental setup**
146 The experiments reported here were conducted in the Main Channel facility at the St.
147 Anthony Falls Laboratory, University of Minnesota, as part of the StreamLab06 project
148 undertaken by the National Center of Earth-Surface Dynamics [*Wilcock et al.,* 2008].
149 StreamLab06 was an 11 month multi-disciplinary laboratory channel study focused on various
150 aspects of ecogeomorphology in gravel bed streams. Five separate projects were conducted as
151 part of StreamLab06 and an extensive data set was collected including hydraulic conditions
152 (discharge, water slope, bed slope, depth average velocity, and flow field), morphological
153 conditions (bed topography, bar locations and shapes, photo images of the bed), sediment
154 transport characterization (continuous sediment flux, recirculation grain size information), water
155 chemistry (temperature, dissolved oxygen, nutrient concentrations) and biological conditions
156 (heterotrophic respiration, biomass accumulation, nutrient processing rates). For the work
157 presented here, we focus on bed topography and sediment flux data collected in the first of the
158 five StreamLab06 projects, which focused on ground-truth testing of various conventional and
159 surrogate bedload monitoring technologies.
160 The Main Channel is 2.74-m wide and has a maximum depth of 1.8 m. It is a partial-
161 recirculating channel with the ability to recirculate gravel while the water flows through the
162 channel without recirculation. Water for the channel was drawn directly from the Mississippi
163 River, with a maximum discharge capacity of 8000 l/s. Water discharge was controlled by a
164 sluice gate situated at the head-end of the facility while flow depth was regulated by a sharp-
165 crested weir located at the downstream end of the channel. The channel has a 55-m long test
166 section and in the experiments reported here a poorly sorted gravel bed extended over the last 20
167 meters of this test section. Short, 0.4m high bulkhead walls were located upstream and

168 downstream of the test section and served to contain the gravel bed material. The gravel used in
169 these experiments had a broad particle size distribution characterized by d_{50} =11.3 mm, d_{16} = 4.3
170 mm and d_{84} = 23.1 mm (see also *Fienberg et al.*, 2008). The thickness of the gravel bed at the
171 start of run was approximately 0.45 m.

172 The Main Channel was equipped with a sediment flux monitoring system that provided
173 the ability to collect high resolution, long duration data sets of sediment transport dynamics using
174 field-scale gravel particle sizes and transport rates. The sediment flux and recirculation systems
175 were co-located in the channel at the downstream end of the 20-m test section. The flux
176 monitoring system was composed of five adjacent, identical aluminum weighing pans (positioned
177 0.54 meters apart) that spanned the width of the channel and independently measured the
178 submerged weight of the gravel intercepted by the bedload trap (see Fig. 1). Each pan could
179 accommodate up to 76-mm-diameter particles and hanged from an aluminum frame that
180 extended from its sides to a load cell connected to the ceiling above the Main Channel (see Fig.
181 2). The system used load cells manufactured by Interface Advanced Force Measurement (SM-
182 250) that had a capacity of 113 kg and were accurate to ±45 gram-force**.** As a safety margin to
183 avoid exceeding the capacity of the weighing pan system, the pan rotation that voided each bin's
184 contents was triggered at a user-specified net weight, which in our case was set to 20 kilogram-
185 force (kg-f).

186 Removable stainless steel cover plates with 45-cm by 15-cm slots served to funnel the
187 intercepted bedload downward into the pans. The pans (also referred as drums) were constructed
188 of aluminum and had three radial baffles welded to a common 3.8-cm diameter hub and to two
189 81.3-cm diameter end plates. They were oriented horizontally and transverse to the channel under
190 the sediment trap. The three radial baffles formed two adjacent 120-degree "V"-shaped bins,
191 each of which had a capacity of 62 liters. The submerged weight of sediment in a bin at
192 maximum capacity was 62 kg-f. Each pan operated independently using a tipping-bucket
193 arrangement with "tips" consisting of alternating clockwise and counterclockwise 120-degree

194 rotations. When the sediment mass in a pan reached a specified threshold, an air cylinder either
195 extended or retracted, causing the pan to rotate 120 degrees. This action resulted in dumping the
196 contents of one bin and repositioning the adjacent empty bin under the funnel to continue
197 collecting bedload. In this manner, all bedload was continuously captured and weighed in the five
198 independently operating pans.
199 Bed load material that was transported out of the test section fell by gravity into the pans and
200 incrementally added to the weight of the pan which was recorded every 1.1 sec. Material dumped
201 out of the pans was collected in a large hopper located underneath the pans, which also served
202 as the material source for the recirculation system. The rate of gravel removal out of this hopper,
203 and delivery to the upstream end of the channel via a large pump, was manually set by adjusting
204 the rotation speed of a large helix, which served to push gravel laterally out of the hopper and
205 into the recirculation line. In this way, the collection hopper and helix served to buffer small
206 fluctuations in sediment flux out of the test section, providing a more steady "feed-type" delivery
207 of sediment to the upstream end. Because the physical size of the collection hopper was finite,
208 the auger speed (and hence upstream input sediment feed rate to the test section) was manually
209 adjusted periodically to maintain storage in the hopper. In other words, an auger rate set too high
210 could potentially remove material faster than the test section would deliver resulting in emptying
211 of the hopper. Conversely, an auger rate set too low would result in overfilling of the hopper. We
212 used periodic visual observations of the fill level in the collection hopper to inform our manual
213 adjustments of the auger speed. Slight adjustments to auger speed were necessary every 30-60
214 min and very rarely did the system collection hopper empty or overfill meaning that the feed rate
215 out of the collection hopper was in balance with the long-term flux of bedload out of the test
216 section.
217 The experimental setup also included five stationary 2.5-cm diameter, submersible sonar
218 transducers deployed 0.95-m below the water surface and 0.95-m upstream of each pan. The
219 sonar transducers, mounted to the end of rigid 1.5-cm steel tubes and directed perpendicular to

220 the bed, were used to collect continuous temporal bed elevation information upstream of the each
221 pan. Sonar data was sampled at every 10sec with a vertical precision of ~1 mm. The acquisition
222 times for the bed elevation and sediment accumulation data were based on precisely
223 synchronized clocks allowing the two data sets to be analyzed together. Water temperature was
224 also measured using YSI thermistor capable of measuring up to +/-0.1^{o}C. Water temperature for
225 the two runs studied in this research averaged 3.0 ^{o}C.

226 Measurements of bed elevation and sediment transport were taken over a range of
227 discharges corresponding to different bed shear stresses. Bed shear stress is often characterized in
228 terms of the dimensionless Shields stress, τ_b^*. For steady, uniform flow it may be approximated
229 as $\tau_b^* = h_R S / R d_{50}$, where h_R and S are the hydraulic radius and channel slope, respectively, and R
230 = 1.65 is the relative submerged density of silica. In the analysis presented here, we report on two
231 different discharges: a low discharge case, with a discharge of 4300 l/s, corresponding to a
232 dimensionless bed stress of about twice the critical value (Shields stress, τ_b^* = 0.085 using
233 median diameter) and a high discharge, 5500 l/s, corresponding to a bed stress about five times
234 the critical value (Shields stress, τ_b^* = 0.196) – see Table 1 for relevant hydraulic parameters.
235 (Note that the critical Shields stress (also known as Shields number) was estimated to be 0.047
236 [*Meyer-Peter and Müller*, 1948]).

237 For both bed stress conditions, the channel was allowed to run prior to data collection
238 such that a dynamic equilibrium was achieved in transport and slope adjustment of the water
239 surface and bed. Determination of the dynamic equilibrium state was evaluated by checking the
240 stability of the 60 min average total sediment flux at the downstream end of the test section.
241 Using the pan accumulation data, the acquisition software computed a 60 min mean of sediment
242 flux in all five pans. Dynamic equilibrium was reached when variation in this value became
243 negligible. In other words, when the average of the previous 60 min of instantaneous flux values

computed from the pan data stabilized, we determined the channel to be in dynamic equilibrium and proceeded with formal data collection and sampling.

The bedload sediment accumulation series and the corresponding bed elevation series were then recorded over a span of approximately 20 hrs for each experiment. Fig. 3 (a) and (b) display the time series of sediment accumulation over 2 min and 10 min intervals respectively for pan 4, and Fig. 3(c) the corresponding bed elevation series (recorded by the sonar transducer immediately upstream of pan 4) for the low discharge conditions over a period of 10hrs. Fig. 4 shows the same series for the high discharge conditions. Considering the bed elevation series, it can be observed that the low bed stress run (Fig. 3c) produced a channel bed with only limited topographic variation, i.e. without obvious large scale structures in the bed (the standard deviation in the bed is 10.1 mm**,** compared to a d_{50} grain size of 11.3mm). However, the higher stress run (Fig. 4c) generated substantial bed variability at large scale in the form of dunes, with intermediate to particle-scale fluctuations superimposed on these larger-scale features. In this study we focus on comparing these two runs using the multiscale analysis techniques to be described in section 3.

2.1. Sources of error in the data

One source of error in the accumulated sediment series was the tipping events of the pans. To account for this, the raw sediment accumulation data were pre-processed prior to the analysis presented here. The pre-processing involved removal of pan dumping events from the data and translating the data set into a continuous accumulation of sediment time series for each pan over the duration of the experiment. A single tipping event required the removal of no more than eight data points (~8.8 sec) from the record. To get the final time series of accumulated sediment transport, the time series prior to the tipping event was left unchanged, the tipping event was removed from the series, and all subsequent points were shifted backwards in time to create a

continuous time series as though the tipping event never occurred. Overall, the data affected by the pan tipping constituted less than 0.15% of the total data record and is, thus, negligible.

There were other sources of error however. Sediment accumulation data in the pans should increase monotonically, when corrected for tipping of the scales as discussed above. At the resolution of our measurements (approximately 1 sec), however, sediment accumulation showed negative excursions which would imply negative bed load flux, which is not physically possible given the experimental setup (see Fig. 3 in *Fienberg et al.,* 2008). These errors have been attributed to (1) the fluctuating water surface over the pan, (2) the natural oscillation of the pans after being hit by the falling gravel, and (3) to the vibration caused by the large gravel recirculation pump which was placed near to the pans. This error makes the raw sediment data at small time scales (from 1 sec up to approximately 1-2 min accumulations) unusable. As a check, we computed distributions of sediment flux values averaged over different time scales and found that data averaged over less than two minutes showed negative values, supporting the contention that scales smaller than two minutes are error prone. Also, although there were five pans, Pans 1 and 5 (Fig. 1) were not used in order to avoid data potentially impacted by wall effects.

Bed elevation data were substantially less error prone, due to the acoustic (rather than mechanical) nature of the measurements. Our multiscale analysis showed a small noise regime which was only a small factor larger than the sampling interval of 10 sec.

3. Roughness, Intermittency and Statistical Scaling

3.1 Characterizing Signal Roughness and Intermittency

Previous authors [e.g. *Gomez et al.*, 1989; *Ancey et al.*, 2006] have observed and documented high fluctuations in bed load sediment transport rates or particle counts at short time-scales, and have described these series as "intermittent". In these and other studies it has also been noted that as flow rate increased, the sediment transport was seen to be "smoother" or more continuous, whereas at low flow rates it was "rougher" or more "bursty". These terms have

295 been used in a qualitative way to describe the presence (or absence) of sudden bursts of sediment
296 or high fluctuations at short time-scales that arise from the stochastic nature of the transport and
297 the collective behavior of particle dynamics.

298 In this paper the "roughness" and "intermittency" of the sediment transport series are
299 mathematically defined, allowing a more precise quantification of the nature of the fluctuations
300 in bed load sediment at small time scales. A mathematical characterization of the strength of
301 local fluctuations in a function $X(t)$ is given by the Hölder or singularity exponent $h(t_0)$,
302 defined at any point t_0 to be the largest exponent such that:

303 $$\left|X(t) - X(t_0)\right| \le C\left|t - t_0\right|^{h(t_0)}, \quad \text{as } t \to t_0 \tag{1}$$

304 where C is a constant. This definition holds for $0 \le h \le 1$, but it can be generalized to $h > 1$, as
305 will be discussed in section 3.3 [see also *Muzy et al.*, 1994]. The Hölder exponent gives a local
306 measure of the smoothness or degree of differentiability of the function $X(t)$: a value of
307 $h(t_0) \ge 1$ indicates that the function is smooth at t_0, in the sense that it is at least once-
308 differentiable at the point t_0, whereas a function with $h(t_0) = 0$ is so rough that it is discontinuous
309 at that point. Between these extremes, a value of $0 < h(t_0) < 1$ means that the function is
310 continuous but not differentiable at t_0, with a higher h value (closer to 1) implying that the
311 function is "smoother" or more regular, and a lower h value (closer to zero) implying that the
312 function is "rougher" or more irregular.

313 Having established a measure of local (point-wise) roughness in a signal, it is natural to
314 ask what kind of $h(t_0)$ values are present in an observed time-series, and how they are
315 distributed. If we denote the set of all points in the function $X(t)$ with a particular value of
316 Hölder exponent h as:

317 $$\Omega(h) = \left\{t_0 : h(t_0) = h\right\}, \tag{2}$$

318 then, in general, for a multifractal function these sets of points are interwoven fractal sets whose
319 distribution can be characterized by the so-called singularity spectrum $D(h)$, defined as

320 $$D(h) = Dim_H\left(\Omega(h)\right) \tag{3}$$

321 where Dim_H is the Hausdorff dimension of the fractal set [e.g. *Schroeder et al.*, 1991]. In other
322 words, the singularity spectrum $D(h)$ describes the relative frequency of occurrence of local
323 abrupt fluctuations (singularities) with strength h. In a one-dimensional function like a time
324 series, the value of h corresponding to the peak of the singularity spectrum indicates the most
325 frequently occurring singularity or fluctuation strength. (Note that if $D(h)$ is symmetric, which is
326 a good approximation for most signals, then this value characterizes the "average roughness" of
327 the signal as it coincides with the arithmetic mean of the local singularities h.) The range of h
328 over which $D(h) \geq 0$, or the spread of the singularity spectrum, reflects the temporal
329 heterogeneity of the local singularities, i.e., it measures the degree of clustering in the abrupt
330 local fluctuations of various strengths. Simply put, a signal with a wide $D(h)$ will have sparse
331 regions where the strength of the local fluctuations is much greater than (or much less than) the
332 mean fluctuation strength, and hence will display infrequent but exceptionally large "bursts" at
333 small scales embedded within bursts of lesser strength, i.e. the signal will be very "intermittent".
334 On the other hand, a $D(h)$ spectrum which is just a spike, i.e., $D(h) = 1$ at $h = H$ and zero
335 elsewhere, indicates a signal which exhibits one strength of singularity only, H also called the
336 Hurst exponent, which is homogeneously distributed throughout the signal (in this case the signal
337 has zero intermittency). It is noted that H, which is a local measure of variability, provides
338 different information than the standard deviation of a signal, which is a global measure of
339 variability; in other words two signals with the same standard deviation can have considerably
340 different values of H (e.g., see *Turcotte*, 1997).

341
342 *3.2 Multiscale analysis*

While the spectrum of singularities $D(h)$ can be used to describe the "roughness" and "intermittency" of a signal, it can be difficult to estimate it directly from the data. An interesting mathematical result (the so-called multifractal formalism, *Parisi and Frisch*, 1985; *Muzy et al.,* 1994) establishes that $D(h)$ relates to how the probability density function (pdf), or equivalently the statistical moments, of the signal fluctuations changes with scale. Let the fluctuation $S(t_0, a)$, at any time t_0 and scale a, be defined as

$$S(t_0, a) = X(t_0 + a) - X(t_0), \tag{4}$$

and the statistical moments of the absolute values of these fluctuations by

$$M(q, a) = \left\langle \left| S(t_o, a) \right|^q \right\rangle \tag{5}$$

where $< \cdot >$ denotes expectation over time. For a process that exhibits statistical scale invariance, the statistical moments of the fluctuations behave as a power-law function of scale:

$$M(q, a) \sim a^{\tau(q)}, \tag{6}$$

where $\tau(q)$ is the so-called spectrum of scaling exponents and is a function of the moment order q. Thus if the series exhibits scale invariance, the function $\tau(q)$ completely describes the manner in which the statistical moments of the pdf of fluctuations varies with scale.

It is the scaling function $\tau(q)$ that can be used to retrieve the spectrum of singularities $D(h)$. The precise transform between these two representations is given by the Legendre transform [*Parisi and Frisch*, 1985; *Muzy et al.,* 1994]:

$$D(h) = \min_q [qh - \tau(q) + 1] \tag{7}$$

In this way the spectrum of singularities describing the average roughness and intermittency of the signal can be estimated through the scaling properties of the statistical moments of the signal fluctuations.

3.3 Generalized Fluctuations and the Wavelet Transform

Although the fluctuations $S(t_0, a)$ of a time series can be computed by directly taking the first order increments, as in equation (4), calculating the statistical moments in this way (which gives rise to the so-called structure function approach) has some limitations. Firstly, these fluctuations can be corrupted by small-scale noise (since observations are used directly without local smoothing); in addition, they do not remove higher order non-stationarities (it is easy to show that the first order increments remove only constant-level trends); and finally, they cannot estimate singularity strengths $h > 1$. To overcome these limitations, the continuous wavelet transform can be used to define generalized fluctuations in the time series (e.g., see *Arneodo et al.*, 1995; *Jaffard,* 1997; *Venugopal et al*., 2006a; and *Lashermes and Foufoula-Georgiou*, 2007). In this framework we redefine the (generalized) fluctuations $S(t_0, a)$ to be

$$S(t_0, a) = \int_{-\infty}^{\infty} \psi_{a,t_0}(t) X(t) dt \,, \tag{8}$$

where $\psi_{a,t_0}(t)$ is a "differencing function", as for example, the first derivative of a Gaussian function. In particular ψ_{a,t_0} is a wavelet resulting from shifting and scaling a mother-wavelet $\psi(t)$, such that,

$$\psi_{a,t_0}(t) = \frac{1}{a}\psi\left(\frac{t - t_0}{a}\right) \tag{9}$$

where t_0 is the location and a is the scale parameter. For the continuous wavelet transform to be invertible, the mother wavelet must satisfy the invertibility condition $\int_{-\infty}^{\infty} t\psi(t)dt = 0$ i.e., it must

have a zero mean (which makes it a kind of local differencing function e.g., see *Mallat*, 1998, or *Kumar and Foufoula-Georgiou*, 1997). A commonly used mother wavelet is the family of Gaussian wavelets defined as the N-order derivatives of a Gaussian function $g_0(t)$, i.e., $g_N(t) = \frac{d^N}{dt^N} g_0(t)$, modulus a proper multiplicative factor to ensure correct normalization. Defining the fluctuations $S(t_0, a)$ using the first order derivative of the Gaussian function can be seen as computing first order increments of the series after the series has been locally smoothed with a Gaussian kernel or, equivalently, as computing first-order increments and then performing a smoothing (weighted averaging). (This can be easily deduced from the convolution theorem; see also *Lashermes et al.*, 2007.) Similarly, defining multiresolution coefficients using $g_N(t)$ can be considered as smoothing the series with a moving Gaussian window, followed by N-th order differencing (the standard deviation of the Gaussian function determines the "scale" at which the smoothing and thus differencing is done; see *Lashermes et al.*, 2007). The smoothing operation removes the noise and the higher order differencing removes nonstationarities from the signal, rendering the wavelet-based generalized fluctuations appropriate for characterization of statistical scaling (e.g., see *Muzy et al*., 1994).

One property that should be considered when choosing an appropriate mother wavelet for defining the mutiresolution coefficients is the number of vanishing moments. Note that the mother wavelet is said to have N vanishing moments if $\int_{-\infty}^{\infty} t^k \psi_o(t) dt = 0$ for $0 \le k < N$. The Gaussian wavelet $g_N(t)$, defined above as the N-th derivative of the Gaussian, can be easily shown to have N vanishing moments. Defining multiresolution coefficients with a mother wavelet which has N vanishing moments can be shown to remove from the series an additive polynomial trend of degree less than N (e.g., see *Kumar and Foufoula-Georgiou*, 1997). Therefore, the wavelet-based multiscale analysis proposed here renders the fluctuation series

410 stationary if one chooses a wavelet with more vanishing moments than the degree of
411 nonstationarity in the data. In practice, the degree of nonstationarity of the data series is not
412 known in advance, so one applies the wavelet transform $g_N(t)$ with increasing values of N until
413 the results of the analysis do not vary with *N*: this will imply that the order has been chosen large
414 enough to remove any nonstationarities. The correct selection of multiresolution coefficients is
415 important for a meaningful multifractal analysis as has been recently demonstrated in *Lashermes*
416 *and Foufoula-Georgiou* (2007). For example, using standard fluctuations (first order differences)
417 to analyze a non-stationary signal will result in a spurious estimate of $H = 1$ misleading one to
418 assume that the signal is smooth and differentiable.

419 In this study, the fluctuations, $S(t_0, a)$, of the bed load sediment and bed elevation series
420 at various scales were computed using the wavelet transform (equation (8)) with the wavelet
421 $g_3(t)$, since this was the lowest order wavelet able to remove all nonstationarities from the
422 sediment transport series (a lower order wavelet g_2 proved sufficient for the bed-elevation series
423 but the use of the higher order wavelet g_3 does not alter the results; this will be discussed more
424 in section 4). The moments $M(q, a)$ were then estimated using equation (5), and the scaling
425 exponents $\tau(q)$ computed from the log-log linear relationships (equation 6) over the scaling
426 range. This in turn allowed the calculation of the singularity spectrum $D(h)$ via equation (7).

427
428 *3.4 Scale dependence of the pdf of the fluctuations*
429

430 The scaling exponents $\tau(q)$ are not only of interest for calculating the singularity
431 spectrum $D(h)$, but also for describing how the pdf of the fluctuations depends on scale. As was
432 discussed earlier, the statistical moments $M(q, a)$ in equation (5) describe how the fluctuations
433 of a process change with scale and, for a scale-invariant process, this change is captured in the
434 $\tau(q)$ curve. In the case of simple scaling, the scaling exponent function is linear in moment

435 order, i.e. $\tau(q) = qH$ for some constant H (called the Hurst exponent), which can be shown to
436 imply that the pdf of the fluctuations at scale a, $P_a(S) \equiv P(S(t,a))$, is related to the pdf at another
437 scale a' by

438 $$P_{a'}(S) = \left(\frac{a}{a'}\right)^{-H} P_a\left(\left(\frac{a}{a'}\right)^{-H} S\right) \tag{10}$$

439 [e.g., see *Arneodo et al.*, 1997 and *Venugopal et al.*, 2006a]. Note that the normalizing factor
440 $\left(\frac{a}{a'}\right)^{-H}$ is a deterministic kernel that depends on H and the ratio of scales (not each scale
441 individually). As this type of statistical scaling behavior is controlled by a single parameter only,
442 it is referred to as monoscaling. Note that equation (7) implies that in the monoscaling case
443 $D(h) = \delta(h - H)$, i.e. the only Hölder exponent with dimension greater than zero is $h = H$, and
444 the function is completely uniform in its roughness i.e., not intermittent, at small scales.

445 In the more general case of multiscaling, the scale invariance relation (equation 6) still
446 holds, but $\tau(q)$ is not linear but a concave function of the moment-order q. In this case, the pdf
447 of the fluctuations does not maintain its shape between two different scales, but changes
448 continuously via convolution with a kernel that depends on the ratio of scales [*Arneodo et al.*,
449 1999b, *Venugopal et al.*, 2006a]. The generalization of equation (10) for multifractals is obtained
450 [*Castaing et al.*, 1990] by considering that H is not a constant but has a probability density
451 function $\rho(h)$. In this case, the expression (10) becomes:

452 $$P_{a'}(S) = \int_{-\infty}^{\infty} \rho(h)\left(\frac{a}{a'}\right)^{-h} P_a\left(\left(\frac{a}{a'}\right)^{-h} S\right) dh \qquad \text{for } a' < a \tag{11}$$

453 In general, the pdf of the fluctuations is expected to widen and have fatter tails as the scale
454 decreases. In turbulence for example, the above transformation renormalizes the almost Gaussian
455 pdf of turbulent velocity fluctuations at very large scales to a thick tailed pdf at small scales. It is
456 noted that the probability density involved in the renormalization of the pdfs is related to the

457 spectrum of singularities $D(h)$, $\rho(h) \propto a^{-D(h)}$, and reflects the presence of Hölder exponents of
458 various strengths which are inhomogeneously distributed throughout the signal (see *Frisch*
459 [1995] and also *Venugopal et al.* [2006a] for a discussion of the equivalency of the geometrical
460 and statistical interpretations). The pdf rescaling of (11) can be expressed in a convolution form
461 as

462 $$P_{a'}(S) = \int_{-\infty}^{\infty} G_{aa'}(u) e^{-u} P_a\left(e^{-u} S\right) du \qquad \text{for } a' < a \qquad (12)$$

463 where $u = h\ ln(a/a')$ and $G_{aa'}(u) = \rho\left(\frac{u}{\ln(a/a')}\right) / \ln(a/a')$. This implies that the pdf at scale a'
464 can be expressed as a weighted sum of dilated pdfs at larger scales $a > a'$. The kernel $G_{aa'}(u)$ is
465 called the propagator and can be estimated from the data (see *Castaing et al.*, 1990 for the theory
466 and *Venugopal et al.*, 2006a for an application to high resolution temporal rainfall series). Once
467 the propagator is known, a known pdf at any scale can be used to derive the pdf at any smaller
468 scale via equation (12).

469 To gain better insight into how the $\tau(q)$ (or $D(h)$) curve controls the pdf change over
470 scales, let us consider the coefficient of variation, C_v, which is the ratio of the standard deviation
471 to the mean, $C_v = \frac{\sigma}{\mu}$. For a monoscaling process, this ratio would be constant with scale, as both
472 the mean and standard deviation are rescaled equally, as shown by equation (6). In a multiscaling
473 situation, however, the increasing width of the pdf leads to C_v increasing with decreasing scale.
474 The precise behavior of C_v with scale can be seen by noting that $C_v^{\,2} + 1 = \frac{M(2,a)}{M(1,a)^2}$, so that for a
475 multiscaling process, equation (6) implies $(C_v^{\,2} + 1) \sim a^{\tau(2)-2\tau(1)}$. In other words, $\tau(2) - 2\tau(1)$
476 characterizes the (second order) relative stretching of pdfs across scales, and its magnitude is also
477 a measure of deviation from monoscaling. Similar relationships can be worked out for higher-

478 moment ratios. As we will see for the sediment transport series, C_v significantly depends on
479 scale, attesting to the presence of multiscaling.
480
481 *3.5 Parameterizing the scaling properties and singularity spectrum*
482
483 While knowing the $\tau(q)$ (or $D(h)$) curve completely characterizes the scale dependence
484 of the pdfs of fluctuations, for practical purposes it is often desirable to parameterize these curves
485 concisely. Assuming an analytic form of the $\tau(q)$ curve, the simplest parameterization for
486 multiscaling is to extend the linear model of $\tau(q)$ used for monoscaling to a quadratic model,
487 that is,

488 $$\tau(q) = c_0 + c_1 q - \frac{c_2}{2} q^2 . \qquad (13)$$

489 In this parameterization, the constant $c_0 = \tau(0)$ is the scaling exponent of the zeroth-order
490 moment, which will be equal to zero if the support of the field under analysis fills the space, as
491 we see for both sediment flux and bed-elevation. This leaves two parameters to describe the
492 (multi)scaling: the parameters c_1 and c_2 control the scaling of all the moments and the change in
493 shape of the pdf with changing scale. The two parameters c_1 and c_2 in (13) can be estimated by
494 fitting a quadratic function to the empirical $\tau(q)$ curve, or via a more robust methodology called
495 the cumulant analysis (see *Delour et al.*, [2001] and *Venugopal et al.* [2006a] for an application
496 to rainfall series).

497 For such a quadratic $\tau(q)$, it can be shown from equation (7) [e.g. *Venugopal et al.*,
498 2006a] that the spectrum of singularities is also quadratic, with

499 $$D(h) = 1 - \frac{1}{2c_2}\left(h - c_1\right)^2 . \qquad (14)$$

500 This shows that the most frequently occurring value of the Hölder exponent (peak of the $D(h)$
501 curve), and hence the mean roughness/smoothness of the function, is given by the parameter c_1
502 (note that $D(h)=1$ and $D(h)$ in (14) is symmetric around c_1). Alternatively, c_2 provides a
503 measure of the spread of the $D(h)$ curve and hence prescribes the degree of intermittency. For
504 this reason, c_2 is referred to as the "intermittency coefficient". The limiting case of $c_2=0$, that is
505 the case of a monofractal, leads to a delta function $D(h)=\delta(h-c_1)$, and hence gives a single
506 Hölder exponent $H=c_1$, (the same exponent H as in equation 10). This means there is no
507 intermittency: the function will have the same degree of local roughness (irregularity)
508 everywhere. For a multifractal ($c_2>0$) however, a range of local fluctuation strengths will be
509 inhomogeneously distributed throughout the signal, with the minimum and maximum Hölder
510 exponents given by $h_{\min/\max}=c_1\mp\sqrt{2c_2}$ (where the $D(h)$ curve crosses below 0). So with
511 increasing c_2 there is a wider range of local fluctuation strengths present in the signal, and hence
512 a greater degree of intermittency.
513
514 **4. Results**
515 *4.1. Sediment transport scaling*
516 Bed load sediment transport fluctuations were analyzed using the multifractal formalism.
517 Fluctuations were computed by applying a differencing filter on the accumulated sediment series
518 $S_c(t)$, i.e., equation (8) with the generic function $X(t)$ replaced now by $S_c(t)$ and using as
519 differencing filters wavelets of increasing order $g_N(t)$, where $N=2$, 3, and 4. It is noted that by
520 using the third derivative of the Gaussian, $g_3(t)$, on the accumulated sediment series, gives
521 fluctuations that represent second order increments of the bedload transport rates, that is, they
522 capture the local rate of change in the sediment transport rates. This filtering guarantees removal

523 of linear trends in the rate of sediment transport series, which, if present, can influence the
524 results. Indeed such rate changes were found present during the 20 hour duration of our data
525 collection (see Fig. 3 in *Fienberg et al*., 2008) and thus the $g_3(t)$ was adopted for our analysis.
526 However, it is noted that the use of lower order wavelets does not significantly change the
527 estimates of the parameters as can be seen from the detailed Table A1 presented in Appendix 1.
528 Having defined the fluctuations, the statistical moments $M(q,a)$ were then computed (equation
529 5), and are shown as a function of scale in Fig. 5, for pan 3 (see Fig. 1). Similar results were
530 obtained for the other pans, except for pans 1 and 5 which suffered from wall effects and showed
531 no good scaling range. Three different regimes can be distinguished for both the low and high
532 discharge: a small-scale regime (scales below 1 min) which is judged to be noise-dominated (see
533 section 2.1); a log-log linear scaling regime in the temporal range of approximately 1 to 10 min;
534 and then a short transitional regime before a leveling-off of the moments is reached. Here we
535 focus on the longer scaling regime between 1 min and 10 min marked by the dashed lines in Fig.
536 5. The scaling exponents of the various moment orders, $\tau(q)$, were estimated using linear
537 regression within this scaling range, and are shown for both discharges in the lower half of Fig. 5.
538 It can be seen that both curves deviate from linear behavior, and hence depart from simple
539 scaling and instead demonstrate multiscaling. The parameters c_1 and c_2 found by fitting the
540 quadratic model (equation 13) to these curves are presented in Table 2, along with a summary of
541 the scaling range and parameters for the other pans for which uninterrupted data were available.
542 It is noted that the quadratic fit is very good and the fitted curves are indistinguishable from the
543 measured points.

544 This scaling of the moments reflects the scaling of the pdf of sediment fluctuations. Fig. 6
545 shows the pdfs of the sediment transport rates (defined as accumulations over an interval divided
546 by the length of that interval) for 2 min and 10 min intervals for both high and low discharge. It
547 can be seen that for both flow conditions, the very skewed and fat-tailed pdf at 2 min changes to

548 a much more symmetrical pdf at 10 min, although in the case of the low flow there is still some
549 skewness present even at the larger sampling time. It is recalled that the parameters c_1 and c_2
550 control this pdf change over scales through the rescaling kernel (equation 12). An easy way to
551 observe the relative narrowing of the pdf with increasing scale is via the coefficient of variation
552 C_v computed from the data, which is plotted in Fig. 7 as a function of scale. The decreasing
553 values of C_v with increasing scale show that the width (spread) of the pdf changes with scale in a
554 different manner compared to the mean (it reduces more quickly) – in agreement with earlier
555 observations by *Kuhnle and Southard* (1988) – and hence reinforces the conclusion that sediment
556 transport fluctuations exhibit multiscaling. A monoscaling function would have constant C_v as
557 mean and standard deviation would rescale similarly – see equation (6).

558 Concentrating on the first order ($q = 1$) statistical moment, which is the mean sediment
559 accumulation in an interval Δt (scale a in the previous notation), we note that it scales as $\Delta t^{\tau(1)}$
560 where $\tau(1) = c_1 - c_2/2$ from equation (13). Using the values of c_1 and c_2 (Table 2) for low flows,
561 it implies that within the scaling range of 1 and 10 min the mean amount of accumulated
562 sediment ($\langle S(t,\Delta t)\rangle$) increases as approximately $\sqrt{\Delta t}$. If one doubles the sampling interval, for
563 example, the amount of sediment accumulated does not double but increases only by a factor of
564 about 1.41. When considering the mean sediment transport rate, ($\langle S(t,\Delta t)/\Delta t\rangle$), the above
565 results imply that it scales as $(\Delta t)^{-0.5}$ or that the bedload transport rate decreases with increasing
566 sampling interval Δt. In other words, doubling the sampling interval results in a transport rate that
567 is approximately 0.7 ($= 1/\sqrt{2}$) times smaller.

568 For high flow rates, the estimated value of $\tau(1)$ is approximately 1.1 (using the values of
569 c_1 and c_2 from Table 2 in equation 13) implying that within the scaling range of 1 and 10 min, the
570 mean amount of accumulated sediment increases as approximately $(\Delta t)^{1.1}$. In this case, doubling
571 the sampling interval increases accumulated sediment by a factor of about 2.1. Considering the

572 mean sediment transport rate, one sees that in the high flow conditions the rate does not remain
573 constant with sampling interval (within the range of sampling interval of 1 to 10 min) but rather
574 slightly increases by a factor of approximately 1.1 ($=2^{0.10}$).

575 The above scaling applies only to the mean and is controlled by the value of $(c_1 - c_2/2)$. As
576 discussed before, our analysis allows one to quantify how higher order statistical moments
577 change with sampling interval in a similar way, for example the second moment about the origin
578 changes as a power law on scale with an exponent $2(c_1 - c_2)$ etc. as dictated by equations (6) and
579 (13).

580 Turning to the singularity spectrum $D(h)$ which characterizes more directly the abrupt
581 fluctuations of the sediment transport series, we recall that it can be computed from the scaling
582 exponents $\tau(q)$ via the Legendre transform (equation (7) or directly from equation (14) using the
583 fitted parameters c_1 and c_2). Fig. 8a shows the $D(h)$ spectrum for the sediment transport in pan
584 3, calculated from the quadratic model fit using the parameters in Table 2. It can be seen that at
585 the low discharge, the sediment transport series is both rougher on the average and more
586 intermittent (lower c_1 and higher c_2, respectively). Conversely, the high discharge case results in
587 a much smoother and less intermittent sediment transport series (higher c_1 and lower c_2,
588 respectively). As it can be seen from Fig. 8a, for low flow rates $h_{\min}$ is approximately zero and
589 $h_{\max}$ is slightly larger than 1. This implies that there are clustered regions in the sediment
590 transport rate series where very high fluctuations are expected over very small intervals (a value
591 of $h = 0$ corresponds to a discontinuous signal) while there are also regions that are very smooth
592 (a value of $h = 1$ corresponds to a signal with continuous first derivative). For high flow rates the
593 values of $h_{\min}$ and $h_{\max}$ are approximately 0.8 and 1.5, implying that the sediment transport series
594 is very smooth overall but there are limited clustered regions where some abrupt fluctuations at
595 small scales are encountered (signal slightly non-differentiable as $h < 1$) while the majority of the

596 series is very smooth. One would expect that these bursts in the sediment transport series are
597 connected to high fluctuations in the bed elevation series which would allow to a lesser or larger
598 degree a collective mobilization of gravel particles. In the next section a multifractal analysis to
599 characterize the roughness and intermittency of bed elevation fluctuations is presented.
600
601 *4.2. Bed elevation scaling*

602 Spatial bed elevation fluctuations have been previously analyzed in terms of their scaling
603 properties, and deviation from simple scaling has been reported [*Nikora and Walsh*, 2004]. Here
604 the temporal fluctuations of bed-elevation were analyzed with the wavelet-based multiscale
605 framework, and scaling of the moments was documented within the range of scales from
606 approximately 1 to 10 min (see Fig. 9), which coincides with the scaling range observed in the
607 sediment transport series and suggests a close link between the dynamics of the two series.
608 Above the characteristic scale of 10 min, the moments leveled off and the statistical quantities
609 became independent of time-scale. The scaling exponents $\tau(q)$ for these moments are shown in
610 Fig. 9, for the high and low discharge experiments. As other authors have reported (e.g., see
611 *Nikora and Walsh*, 2004), a deviation from simple scaling is observed for both discharge rates
612 indicating the presence of temporal heterogeneity in the local roughness (what we have called
613 "intermittency") in bed elevation fluctuations. The parameters c_1 and c_2 fitted to the $\tau(q)$
614 curves of the bed elevation fluctuation series are displayed in Table 3, and the corresponding
615 singularity spectra $D(h)$ are presented in Fig. 8b. Similar to the sediment transport fluctuations,
616 we observe that bed-elevation fluctuations are rougher on an average in the low discharge case
617 than in the high discharge case (c_1 = 0.57 vs. c_1 = 0.68), although to a lesser extent than in the
618 sediment series. However, considering the degree of intermittency in the bed elevation
619 fluctuations, we see that it is higher at the high transport case (a wider $D(h)$ spectrum and a

620 larger c_2 value) with a coefficient of intermittency $c_2 = 0.13$, versus a narrower $D(h)$ and $c_2 =$
621 0.06 in the case of low transport. This is reverse from what is observed in the sediment transport
622 fluctuations (see also Fig. 8a) and calls for an explanation based on further experimentation and
623 mechanistic modeling.
624
625 **5. Discussion**

626 The simultaneous collection of bed load transport and bed elevation data in a field-scale
627 channel is the major strength of the experimental setup used in this work. The large channel
628 geometry, and high temporal resolution of the data, allowed robust statistical analysis over a wide
629 range of temporal scales. Despite the more comprehensive data sets collected as part of the
630 STREAMLAB-06 experiments our analysis here is concentrated on two data sets at two different
631 flow rates, as these are the only data currently available for analysis. The mixed grain size
632 distribution of the feed material, while beneficial for mimicking a natural gravel stream, makes it
633 more difficult to discern the influences of spatial grain size sorting [*Iseya and Ikeda*, 1987;
634 *Kuhnle and Southard*, 1988; *Cudden and Hoey*, 2003; *Frey et al.,* 2003] from those of bed
635 topography and collective grain motion [*Gomez et al.,* 1989; *Jerolmack and Mohrig*, 2005; *Ancey*
636 *et al.,* 2008] on sediment transport fluctuations. Also, for this experiment we do not have any
637 data regarding armoring of the stream bed over the duration of the experiments, or the grain size
638 distributions of individual sediment pulses. With these limitations in mind, in this section we
639 place our experimental results and analysis in the context of laboratory and field studies of
640 sediment transport fluctuations in uniform and mixed-grain size channels.

641 The multiscaling analysis demonstrates how the statistical moments of bed load transport
642 rate depend on the time scale of observation. To illustrate, we first examine the behavior of the
643 mean transport rate (the first moment). Estimating mean sediment transport rate is essential for

644 measuring the material flux through a river, and for model input and/or calibration. For the low
645 discharge run (τ_b^* = 0.085), mean transport rate decreased with sampling interval, while at higher
646 discharge (τ_b^* = 0.196), the trend reversed: mean transport rate slightly increased with sampling
647 interval over a comparable time range. A similar trend was discovered by *Bunte and Abt* [2005],
648 who studied the effect of sampling interval on bed load transport rates measured using Helley-
649 Smith samplers deployed in a mixed gravel-cobble stream of a size comparable to our
650 experiments. They found that in moderate to high flows (50% bankfull to almost bankfull
651 conditions) 2 min sampling led to an average transport rate 2 to 5 times lower than that found
652 with 10 min sampling. However, at lower flows (close to the incipient gravel motion) 2 min
653 sampling overestimated the transport rates at 10 min sampling by a factor of almost 3. Although
654 not directly comparable, the trends observed are qualitatively the same as our experiments (Fig.
655 10). *Bunte and Abt* [2005] attribute the higher discharge trend to the effect of large but infrequent
656 transport events associated with the crests of bed forms: small sampling intervals underestimate
657 mean transport because they are likely to miss these events. They suggest that the reversal in
658 trend for the low discharge observations is the result of sampling and computational difficulties,
659 rather than a "real" effect. Our high-resolution experiments demonstrate that this trend reversal
660 might in fact be real.

661 It is stressed that it is difficult to quantitatively compare the field results to our laboratory
662 experiments, due to differences in transport and lack of the detailed field data. *Bunte and Abt*
663 [2005] do not report Shields stress, but they report that their low flow observations correspond to
664 incipient sediment motion which is supported by our calculation of their critical Shields stress
665 ($\tau^* = 0.047$) using their reported bankfull flow characteristics. Our low flow experiment had a
666 Shields stress almost twice the critical value, making it comparable in terms of stress to their
667 moderate flow observations. Thus it seems that in both the study of Bunte and Abt and our study,
668 suggest a reversal in trend, from decreasing to increasing mean transport rate with sampling

669 interval, as bed stress increases. The fact that the reversal appears to occur for different stress
670 values in the field and the laboratory may be the result of the multiple intricacies of sediment
671 transport and grain size sorting of heterogeneous mixtures in turbulent flows. Clearly,
672 experiments systematically document how the statistics of transport rate change with bed stress
673 over a wide range of values would be helpful in illuminating this point.

674 Several field and laboratory experiments have documented sediment transport
675 fluctuations in mixed-grain size sediments. *Iseya and Ikeda* [1987] found strong longitudinal
676 grain size sorting in mixed gravel and sand experiments, which caused periodic fluctuations in
677 transport rate due to changing local sediment supply. Such periodic pulses in gravel-sand
678 mixtures have also been reported by *Kuhnle and Southard* [1988] and *Frey et al.* [2003]. These
679 experiments cannot be directly compared to our results, however, because they had limited bed
680 topography and/or antidunes, while our experimental channel allowed for the growth of large bed
681 forms in subcritical flow. These studies suggest that the creation and destruction of sediment
682 patches of different grain sizes [see also *Cudden and Hoey*, 2003] due to longitudinal grain size
683 sorting within the channel likely contributed somewhat to the observed transport fluctuations in
684 our experiments, but are not capable of explaining all of this variability.

685 Sediment transport rates became smoother and less intermittent with increasing bed stress
686 in our experiments, in agreement with previous observations. Near the threshold of motion,
687 grains are in partial transport because local bed stress fluctuates above and below the threshold
688 value. These turbulent fluctuations, along with grain-to-grain interactions at the bed, result in
689 intermittent and collective motion of grains, leading to nonrandom transport rate fluctuations
690 with heavy tails [*Ancey et al.,* 2008]. In a mixed grain size bed, size selective transport often
691 occurs which may enhance this effect [*Kuhnle and Southard*, 1988]. The experiments of *Ancey et*
692 *al.* [2008] demonstrate that such fluctuations can occur even in glass spheres of uniform size,
693 with little or no bed topography. As bed stress is increased such that the local stress fluctuations

694 are always above the critical value, all grains become entrained in the flow as the intermittent,
695 collective motions of grains gives way to continuous transport [*Iseya and Ikeda,* 1987; *Kuhnle*
696 *and Southard*, 1988; *Ancey et al.,* 2008; *Strom et al.,* 2004]. While this effect has been
697 documented qualitatively by previous authors, our results quantify these changes in the statistics
698 of sediment fluctuations with bed shear stress.

699 Bed elevation also became smoother with increasing transport, meaning that the
700 magnitude of high frequency fluctuations at small scales was reduced overall. At low flow
701 conditions, topographic fluctuations were of the order of the grain scale (Fig. 3), supporting the
702 idea that grain-grain interactions (and perhaps longitudinal grain-size sorting) dominated
703 transport fluctuations as described above. With increasing bed stress, and presumably full
704 mobility of all grains in transport based on Shields stress calculations, the bed organized into
705 large-scale bed forms (Fig. 4). Data indicate that higher frequency (smaller-scale) topography,
706 likely representing clusters of grains, became less prevalent at higher flows where bed
707 topography was dominated by dune forms. Interestingly, although the bed became smoother
708 overall from low to high discharge, intermittency increased. In other words, high small-scale
709 frequency fluctuations in bed topography became less prevalent overall, but also less uniformly
710 distributed. This may be due to irregular clusters of grains superimposed on larger scale, more
711 regular dune features. However, observations of grains on the bed were not made and so these
712 ideas remain speculative at this stage. Our experiments highlight the need to simultaneously
713 document bed topography, bed load transport rates and individual particle motions (e.g., as those
714 of *Schmeeckle et al.,* 2001; *Papanicolaou et al.,* 2002; and *Ancey et al.,* 2006) in order to further
715 our understanding of what contributes to transport fluctuations at the smallest to largest scales.

716 The scaling ranges of both transport rates and bed elevation series are similar with a
717 leveling off, or saturation, at approximately the same time scales, indicating that fluctuations in
718 transport are intimately related to bed topography. While the nature of these dependencies is still

719 unclear, a practical result may be obtained. The scale-dependent nature of transport (within 1 and
720 10 min in this study) means that measured rates at different time intervals are not directly
721 comparable. In our experiments, both transport and bed elevation exhibit no time dependence
722 when measured over intervals greater than 10 to 15 min. In other words, if we measure for a
723 period of time that is larger than the timescale associated with the migration of the largest
724 topographic feature, we can obtain mean values for bed topography and transport rate that have
725 no time dependence [*Fienberg et al.,* 2008]. From a practical point of view, this is the mean
726 transport rate one should try to obtain in the field. Measurements of bed topography from a river
727 could be used to determine the upper scaling limit of fluctuations – which determines the
728 timescale over which one should deploy a sampler to obtain a representative "mean" bed load
729 transport value. As discussed by *Fienberg et al.* [2008], this approach is possible in flumes and
730 small streams where the timescale is of the order of tens of minutes. Since the size of bed forms
731 scales with river depth, however, this approach quickly becomes impractical as river size
732 increases – deployment of bed load samplers for long durations can result in overfilling and
733 clogging [e.g., *Bunte and Abt*, 2005], or integrating over changing flow conditions. In this case,
734 determining the scale-dependent nature of transport rate becomes critical.
735
736 **6. Conclusions**
737 In this paper we introduced a formalism, typically used in turbulence studies, to quantify
738 two properties in sediment transport and concurrent bed elevation series: the "average
739 roughness" of the series (depicting the average strength of local abrupt fluctuations in the signal)
740 and the "intermittency" (depicting the temporal heterogeneity of fluctuations of different
741 strength). In the bedload sediment transport rates, we documented the presence of a rougher and
742 more intermittent behavior at low transport conditions (dimensionless bed shear stress of about
743 twice the critical value) transiting to a smoother and less intermittent behavior at high transport
744 conditions (dimensionless shear stress of about five times the critical value).

745 Apart from simply quantifying roughness and intermittency of the sediment transport
746 rates, the results of our analysis provide a framework for quantifying how the probability
747 distribution of sediment transport rates changes with sampling interval and thus have important
748 practical implications. (It is interesting to note that the change of pdf with scale is parameterized
749 in terms of the roughness and intermittency parameters which characterize the burstiness of the
750 series.) Specifically, our analysis demonstrated that the statistics of bedload sediment transport
751 rates depend strongly on scale (sampling interval) and this dependence varies with the discharge
752 conditions. Our results agree with the field observations reported by *Bunte and Abt* [2005] for
753 mean bedload rates and call for a more systematic study to precisely quantify this scale
754 dependence in terms of grain size sorting and bed shear stress. It is noted that the theoretical
755 framework we propose here offers the ability to go beyond the mean and compare the whole
756 probability density function, including extreme values or quantiles, at different scales. This is
757 important for example when the pdf of sediment transport rates has been estimated from data at
758 one particular sampling interval and an extreme exceedance quantile (say, relevant to an
759 ecological smaller-scale functional disturbance) needs to be estimated. Our methodology can
760 bridge this gap in scales and also provide a framework with which comparison of sediment rates
761 sampled with different instruments can be made.

762 A problem of continuous interest in the literature is the relation of microscale (particle-
763 scale) dynamics to the macroscale behavior of sediment transport (e.g., *Drake et al.*, 1988;
764 *Papanicolaou et al.*, 2002; *Schmeeckle et al.*, 2001, 2003; *Ancey et al.*, 2006, 2008, among
765 several others). Although not precisely quantified in this paper, it is worth noting that the multi-
766 scale statistical behavior of sediment transport rates (as quantified here via the signal roughness
767 and intermittency) seems consistent with known particle-scale dynamics. For example, at low
768 flows, a rougher but more temporally homogeneous (less intermittent) bed elevation series was
769 documented, indicative of the dominance of high-frequency localized grain clusters; this bed
770 micro-topography apparently gave rise to sediment transport rates that are almost of equal

771 roughness but are more inhomogeneous in time (more intermittent); see Fig. 8. This might be due
772 to the collective motion of grains responding to local bed stress fluctuating above and below the
773 critical value. It appears that as bed stress increased, grain patches became less prevalent and
774 more irregular (roughness in bed elevations decreased but intermittency increased) as the bed
775 organized into large-scale dunes, and bedload transport became smoother and more
776 homogeneous in time as entrainment of all grains commenced. This speaks for the collective or
777 cooperative behavior of particle movement that has different dynamics at low and high flows and
778 depends on the presence or absence of self-formed structures on the bed [e.g., *Drake et al*., 1988;
779 *Ancey et al.,* 2008].

780 We see our study as a first step in the direction of understanding the scale-dependency of
781 sediment transport rates over the continuum of flow discharge conditions and grain size
782 distributions and relating the statistics of bed elevations to the statistics of bedload sediment
783 transport. More controlled experiments have to be performed and analyzed with different particle
784 sizes (from a single particle size to a broad particle size distribution and for gravel and sand-
785 beds) and a spectrum of discharge rates, to fully characterize the intermittency of bedload
786 sediment transport rates and how it relates to that of the bed elevation fluctuations, and
787 (eventually) to particle-size dynamics. Also, the documented statistical structure of sediment
788 transport rates can be seen as providing an additional model diagnostic that mechanistic models
789 should be able to reproduce, and as such, it is interesting to ask as to whether any known
790 sediment transport model can reproduce the multiscaling characteristics reported in this study.

791

792 **Acknowledgement**

793 This research was inspired by the STREAMLAB-06 experiments conducted at St.
794 Anthony Falls Laboratory as part of an interdisciplinary research agenda set by the National
795 Center for Earth-surface Dynamics (NCED) at the University of Minnesota. NCED is a Science
796 and Technology Center funded by NSF's Office of Integrative Activities under agreement EAR-

797 0120914. We thank Christophe Ancey, Thanos Papanicolaou, and an anonymous reviewer, as
798 well as the associate editor and Michael Church, whose suggestions and constructive comments
799 substantially improved our presentation and refined our interpretations. We also thank Peter
800 Wilcock, Gary Parker and Mark Schmeeckle for stimulating discussions. All computational
801 resources were kindly provided by the Minnesota Supercomputing Institute. The senior author
802 acknowledges support from the Joseph T. and Rose S. Ling Professorship in Environmental
803 Engineering at the University of Minnesota. The StreamLab06 data are available from the
804 authors upon request.
805
806 **References:**
807 Aberle, J., and V. Nikora (2006), Statistical properties of armored gravel bed surfaces, *Water*
808 *Resour. Res.*, 42, W11414, doi:10.1029/WR004674.
809 Ancey, C., T. Böhm, M. Jodeau, and P. Frey (2006), Statistical description of sediment transport
810 experiments, *Phys. Rev. E*, 74(1), Art. No. 011302 .
811 Ancey, C., A.C. Davidson, T. Böhm, M. Jodeau, and P. Frey (2008), Entrainment and motion of
812 coarse particles in a shallow water stream down a steep slope, *J. Fluid Mech.,* 595, 83-114.
813 Arneodo, A., E. Bacry, and J. F. Muzy (1995), The thermodynamics of fractals revisited with
814 wavelets, *Physica A*, 213, 232-275.
815 Arneodo, A., J. F. Muzy, and S. G. Roux (1997), Experimental analysis of self-similarity and
816 random cascade processes: Application to fully developed turbulence data, *Journal De*
817 *Physique II,* 7(2), 363-370.
818 Arneodo, A., N. Decoster, and S. G. Roux (1999a), Intermittency, lognormal statistics, and
819 multifractal cascade process in high-resolution satellite images of cloud structure, *Phys. Rev.*
820 *Letters*, 83(6), 1255-1258.

Arneodo, A., S. Manneville, J. F. Muzy, and S.G. Roux (1999b), Revealing a lognormal cascading process in turbulent velocity statistics with wavelet analysis, *Philosophical Transaction: Mathematical, Physical and Engineering Sciences*, 357(1760), 2415-2438.

Bunte, K., and S. R. Abt (2005), Effect of sampling time on measured gravel bed load transport rates in a coarse-bedded stream, *Water Resour. Res.*, 41, W11405, doi:10.1029/2004WR003880.

Castaing, B., Y. Gagne, and E. J. Hopfinger (1990), Velocity probability density-functions of high Reynolds-number turbulence, *Physica D, 46*, 177–200.

Cudden, J. R. and T. B. Hoey (2003), The causes of bedload pulses in a gravel channel: The implications of bedload grain-size distributions, *Earth Surf. Proc, Landforms*, 28, 1411-1428.

Delour, J., J. Muzy, and A. Arneodo (2001), Intermittency of 1D velocity spatial profiles in turbulence: A magnitude cumulant analysis, *Eur. Phys. J. B*, 23, 243–248.

Dinehart, R. L. (1992), Evolution of coarse gravel bed forms: field measurements at flood stage, *Water Resour. Res.*, Vol. 28, No. 10, Pages 2667-2689.

Drake, T., R. Shreve, W. Dietrich, P. Whiting, and L. Leopold (1988), Bedload transport of fine gravel observed by motion-picture photography, *J. Fluid Mech*., 192, 193-217.

Fienberg, K., A. Singh, D. Jerolmack, J. Marr and E. Foufoula-Georgiou (2008), A Theoretical framework for interpreting and quantifying the sampling time dependence of gravel bedload transport rates, *Proceedings of Bedload Research International Cooperative*, Minneapolis, April 11-14, 2007. (Accepted)

Foufoula-Georgiou, E., and V. Sapozhnikov (1998), Anisotropic scaling in braided rivers: An integrated theoretical framework and results from application to an experimental river, *Water Resour. Res.*, 34(4), 863-867.

Frey, P., C. Ducottet, and J. Jay (2003), Fluctuations of bed load solid discharge and grain size distribution on steep slopes with image analysis*, Experiments in Fluids*, 35, 589-597.

Frisch, U. (1995), *Turbulence: The Legacy of A. N. Kolmogorov*, Cambridge University Press, New York.

Gangodagamage, C., E. Barnes, and E. Foufoula-Georgiou (2007), Scaling in river corridor widths depicts organization in valley morphology, *J. Geomorphol*., 91, 198-215.

Gomez, B., R. L. Naff, and D. W. Hubbell (1989), Temporal variation in bedload transport rates associated with the migration of bedforms, *Earth Surf. Processes Landforms*, 14, 135–156.

Gupta, V., and E. Waymire (1996), Multiplicative cascades and spatial variability in rainfall, river networks, and floods, in *Reduction and Predictability of Natural Disasters*, edited by J. B. Rundle, D. L. Turcotte, and W. Klein, Santa Fe Inst. Stud. Sci. Complexity, vol. 25, Addison-Wesley, Boston, Mass.

Iseya, F., and H. Ikeda (1987), Pulsations in bedload transport rates induced by a longitudinal sediment sorting: a flume study using sand and gravel mixtures, *Geografiska Annaler*, 69 A, 15-27.

Jaffard, S. (1997), Multifractal formalism for functions, *SIAM J. Math. Anal.,* 28(4), 944–998.

Jerolmack, D. J., and D. Mohrig (2005), A unified model for subaqueous bed form dynamics, *Water Resour. Res.*, 41, W12421, doi:10.1029/2005WR004329.

Jerolmack, D. J., and P. M. Sadler (2007), Transience and persistence in the depositional record of continental margins, *J. Geophys. Res*., 112, F03S13, doi:10.1029/2006JF000555.

Kuhnle, R. A., and J. B. Southard (1988), Bed load fluctuations in a gravel bed laboratory channel, *Water Resour. Res.*, 24, 247-260.

Kumar, P., and E. Foufoula-Georgiou (1997), Wavelet analysis for geophysical applications, *Reviews in Geophysics*, 35(4), 385-412.

Lashermes, B., and E. Foufoula-Georgiou (2007), Area and width functions of river networks: New results on multifractal properties, *Water Resour. Res.*, 43, W09405, doi:10.1029/2006WR005329.

871 Lashermes, B., E. Foufoula-Georgiou, and W. E. Dietrich (2007), Channel network extraction
872 from high resolution topography data using wavelets, *Geophys. Res. Lett.*, 34, L23S04,
873 doi:10.1029/2007GL031140.
874 Lovejoy, S., and D. Schertzer (1985), Generalized scale invariance and fractal models of rain,
875 *Water Resour. Res.*, 21, 1233-1250.
876 Lovejoy, S., D. Schertzer, P. Silas, Y. Tessier, and D. Lavallée (1993), The unified scaling model
877 of atmospheric dynamics and systematic analysis in cloud radiances, *Ann. Geophys.*, 11, 119–
878 127.
879 Mallat, S. (1998), *A Wavelet Tour in Signal Processing*, Academic Press, New York.
880 Marani, M., A. Rinaldo, R. Rigon, and I. Rodŕiguez-Iturbe (1994), Geomorphological width
881 functions and the random cascade, *Geophys. Res. Lett*., 21, 2123-2126.
882 Meyer-Peter, E. and R. Müller (1948), Formulas for Bed-Load Transport, *Proceedings*, 2nd
883 Congress, International Association of Hydraulic Research, Stockholm: 39-64.
884 Muzy, J. F., E. Bacry, and A. Arneodo (1994), The multifractal formalism revisited with
885 wavelets, *Int. J. Bifurcation Chaos*, *4*, 245-302.
886 Nikora, V., H. Habersack, T. Huber, and I. McEwan (2002), On bed particle diffusion in gravel
887 bed flows under weak bed load transport, *Water Resour. Res.*, 38, 1081,
888 doi:10.1029/2001WR000513.
889 Nikora, V., and J. Walsh (2004), Water-worked gravel surfaces: High-order structure functions at
890 the particle scale, *Water Resour. Res.*, 40, W12601, doi:10.1029/2004WR003346.
891 Nikora, V., A. N. Sukhodolov, and P. M. Rowinski (1997), Statistical sand wave dynamics in
892 one-directional water flows, *J. Fluid Mech*., 351, 17– 39.
893 Nikora, V., and D. M. Hicks (1997), Scaling relationships for sand wave development in
894 unidirectional flows, *J. Hydraul. Eng.*, 123, 1152– 1156.

895 Papanicolaou, A., P. Diplas, N. Evangelopoulos, and S. Fotopoulos (2002), Stochastic incipient
896 motion criterion for spheres under various bed packing conditions, *J. Hydraulic Engr.*, 128,
897 369-380.
898 Parisi, G., and U. Frisch (1985), On the singularity structure of fully developed turbulence, in
899 *Turbulence and Predictability in Geophysical Fluid Dynamics*, edited by M. Ghil et al., North -
900 Holland, Amsterdam, 84-87.
901 Rinaldo, A., I. Rodriguez-Iturbe, R. Rigon, E. Ijjasz-Vasquez, and R. Bras (1993), Self-organized
902 fractal river networks, *Phys. Rev. Lett.*, 70, 822– 825.
903 Sadler, P. M. (1981), Sediment accumulation and the completeness of stratigraphic sections, *J.*
904 *Geology*, 89, 569-584.
905 Sadler, P. M. (1999), The influence of hiatuses on sediment accumulation rates, *GeoResearch*
906 *Forum*, 5, 15-40.
907 Schmeeckle, M. W., J. M. Nelson, J. Pitlick, J.P. Bennett (2001), Interparticle collision of natural
908 sediment grains in water, *Water Resour. Res.*, 37 (9), 2377-2391.
909 Schmeeckle, M.W., and J. M. Nelson (2003), Direct numerical simulation of bedload transport
910 using a local, dynamic boundary condition, *Sedimentology,* 50 (2) , 279–301
911 doi:10.1046/j.1365-3091.2003.00555.
912 Schroeder, M. (1991), *Fractals, Chaos, Power Laws: Minutes from an Infinite Paradise*, W.H.
913 Freeman, New York.
914 Strom, K., A. N. Papanicolaou, N. Evangelopoulos, M. Odeh (2004), Microforms in Gravel Bed
915 Rivers: Formation, Disintegration, and Effects on Bedload Transport, *J. Hydraulic Engr.*, 133,
916 554-567.
917 Sumer, B. M., L. H. C. Chua, N. S. Cheng, and J. Fredsoe (2003), Influence of turbulence on bed
918 load sediment transport, *J. Hydraul. Eng.*, 129, 585– 596.
919 Turcotte, D. L. (1997), *Fractals and Chaos in Geology and Geophysics*, 2nd edition, Cambridge
920 Univ. Press, New York.

921 Venugopal, V., S. G. Roux, E. Foufoula-Georgiou, and A. Arneodo (2006a), Revisiting
922 multifractality of high-resolution temporal rainfall using a wavelet-based formalism, *Water*
923 *Resour. Res.*, 42, W06D14, doi:10.1029/2005WR004489.
924 Venugopal, V., S. G. Roux, E. Foufoula-Georgiou, and A. Arneodo (2006b), Scaling behavior of
925 high resolution temporal rainfall: New insights from a wavelet-based cumulant analysis, *Phys.*
926 *Let. A*, 348, 335-345.
927 Wilcock, P. R., C. H. Orr, and J. D. G. Marr (2008), The need for full-scale experiments in river
928 science, *EOS, Transactions, Am. Geophys. Union.*, Vol.89, 1.
929 Yarnell, S.M., J.F. Mount, and E.W. Larsen (2006), The Influence of relative sediment supply on
930 riverine habitat heterogeneity, *Geomorphology,* 80, 310-324.
931

Table 1: Hydraulic conditions for the two studied discharges.

Q_w (l/s)	Depth (m)	V (m/s)	h_R (m)	S_w (%)	τ_b*	T_{mean} (^oC)
4300	1.3	1.20	0.67	0.23	0.085	3.5
5500	1.3	1.54	0.67	0.53	0.196	2.7

Variables: Q_w = Design water discharge for the run
Depth = average depth of flow in test section
v = velocity of flow
h_R = Hydraulic radius
S_w = water surface slope
τ_b* = Dimensionless Shields stress (computed using hydraulic radius)
T_{mean} = Mean water temperature

Table 2: Summary of statistical scaling analysis results for the bedload sediment series (see text for definition of variables).

Q (l/s)	Pan	Scaling Range (min)	Shields stress	τ (2) – 2 τ(1)	c_1	c_2
4300	2	1.2-10	0.085	-0.20	0.56	0.14
	3	1.2-10		-0.19	0.49	0.13
	4	1- 8		-0.15	0.47	0.10
5500	2	1-10	0.196	-0.13	1.07	0.09
	3	1-10		-0.16	1.07	0.10
	4	1-10		-0.15	1.12	0.11

Table 3: Summary of statistical scaling analysis results for the bed elevation time series (see text for definition of variables).

Q (l/s)	Probe	Scaling Range (min)	Shields stress	τ (2) – 2 τ(1)	c_1	c_2
4300	4	1-10	0.085	-0.04	0.57	0.06
	5	1-10		-0.06	0.53	0.08
5500	2	0.5-8	0.196	-0.18	0.65	0.12
	3	0.5-8		-0.19	0.68	0.14
	4	0.5-8		-0.20	0.76	0.13

945
946

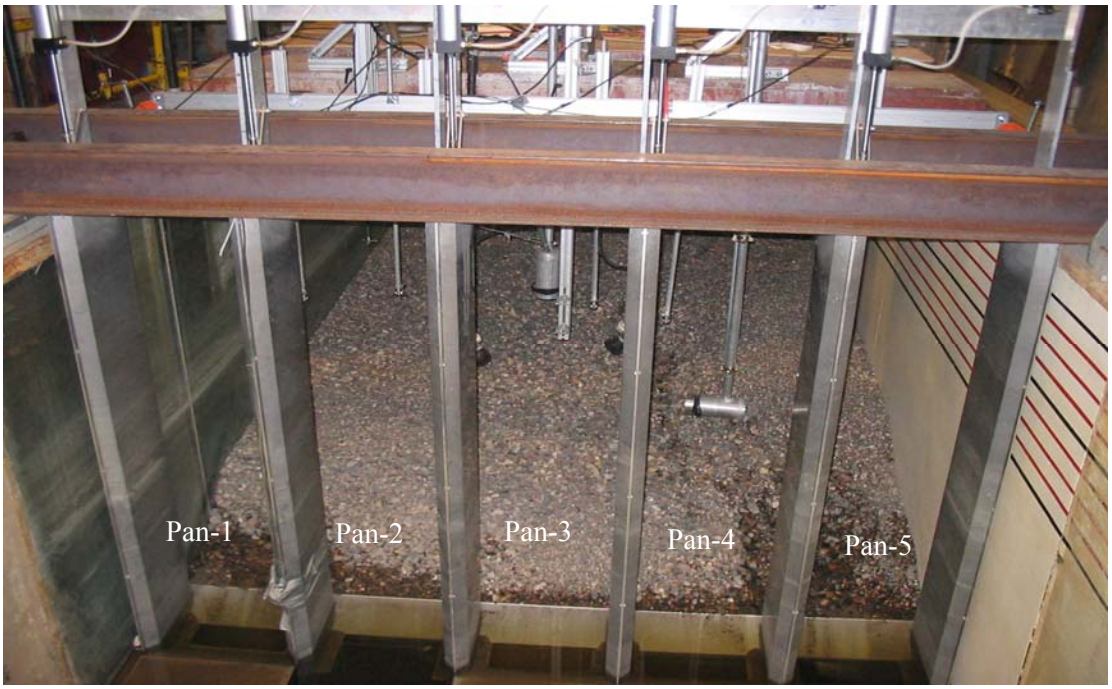

947
948
949

950 **Figure 1:** Weighing pans located at the downstream end of the experimental Main Channel.

951

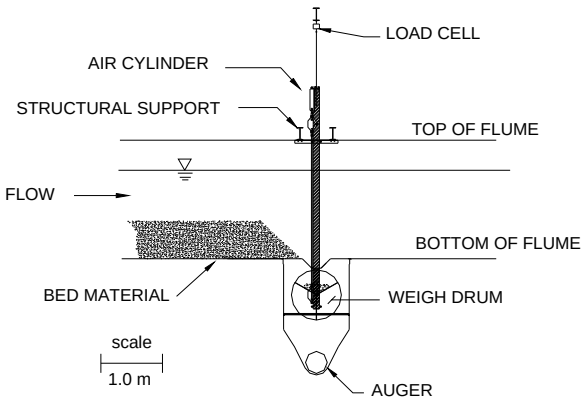

952

953 **Figure 2:** Side view schematic of a pan and sediment recirculation system in the Main Channel.

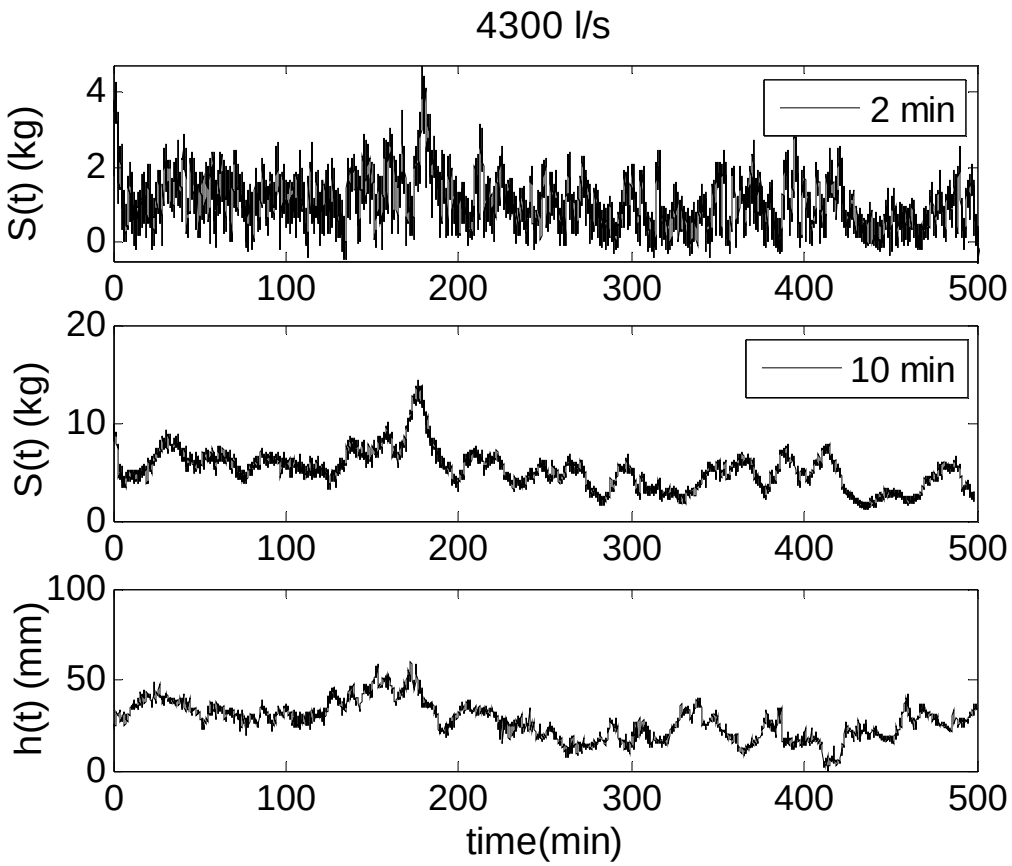

954

955 **Figure 3**: Low transport conditions (flow rate 4300 l/s): Bedload sediment transport series

956 accumulated every 2 min (a), and 10 min (b), and the corresponding series of gravel bed

957 elevations (c).

958

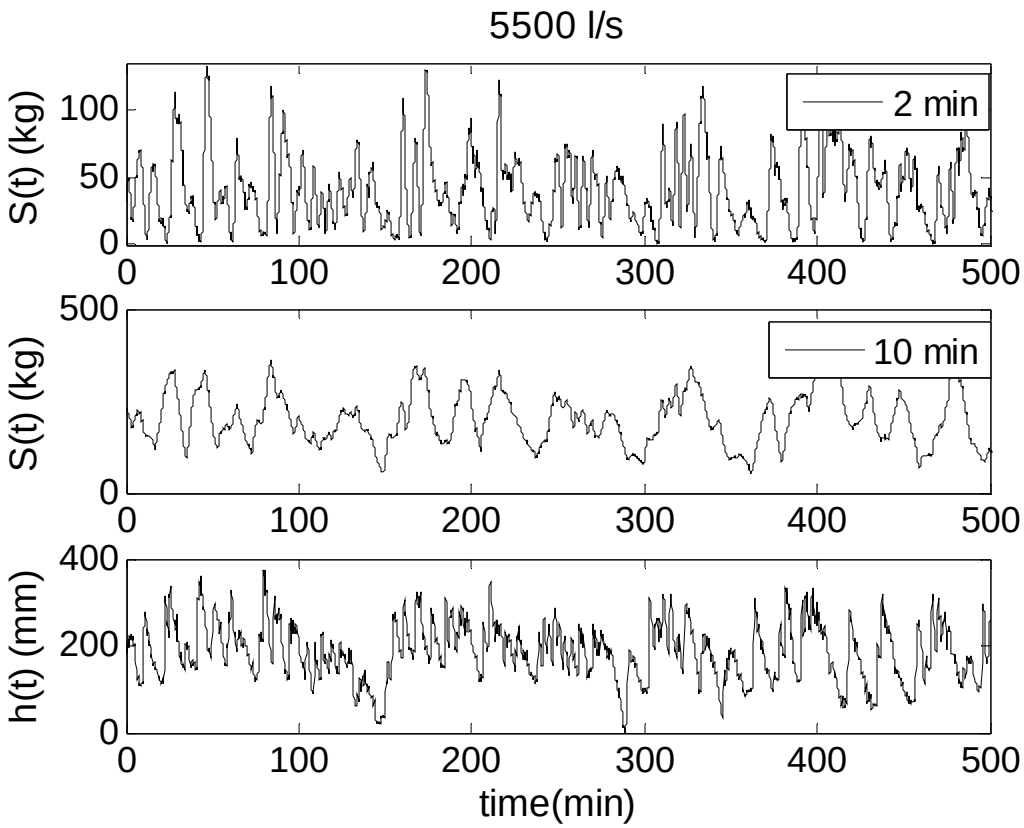

959

960 **Figure 4:** High transport conditions (flow rate 5500 l/s): Bedload sediment transport series
961 accumulated every 2 min (a), and 10 min (b), and the corresponding series of gravel bed
962 elevations (c).

963

964

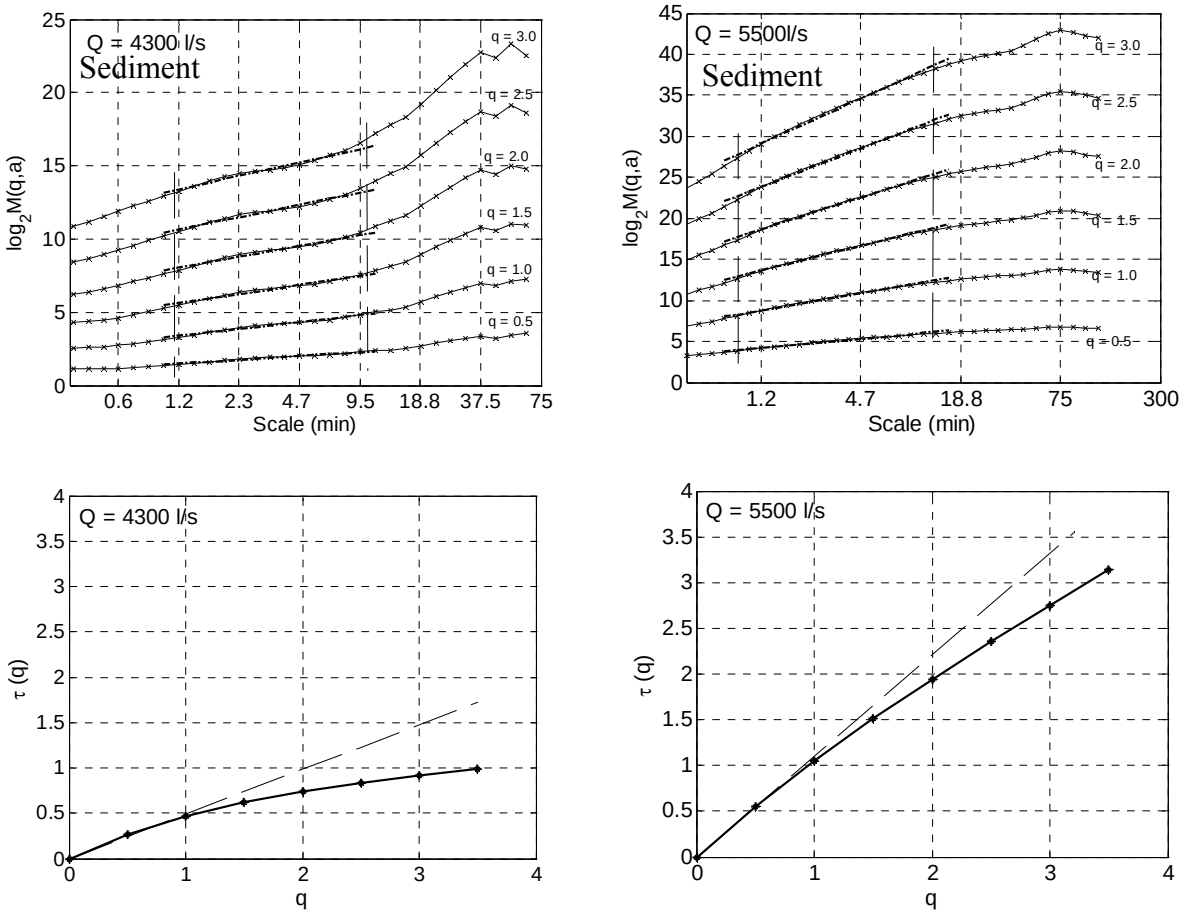

965

966

967

968

969 **Figure 5:** (top) Statistical moments of the fluctuations of the sediment transport series as a

970 function of scale and (bottom) the scaling exponents $\tau(q)$ estimated from the log-log linear

971 regressions within the scaling regions. Notice the deviation of $\tau(q)$ from the linear line

972 establishing the presence of multifractality. (left) For low-transport conditions and (right) for

973 high-transport conditions.

974

975

976

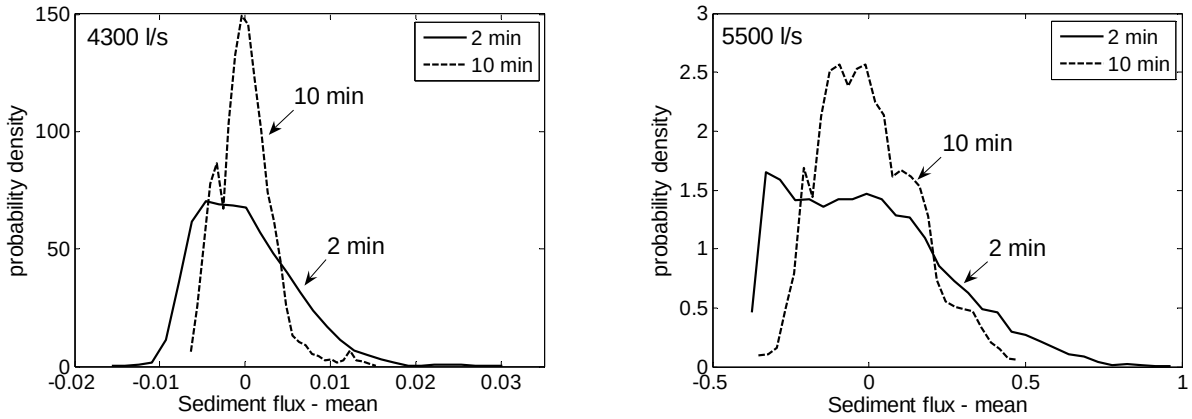

977
978

979 **Figure 6:** Probability distribution functions of the sediment transport rate (flux) for sampling
980 intervals of 2 and 10 min for low (left) and high (right) discharge rates. The probability
981 distributions have been shifted to zero mean for comparison.

982
983
984
985

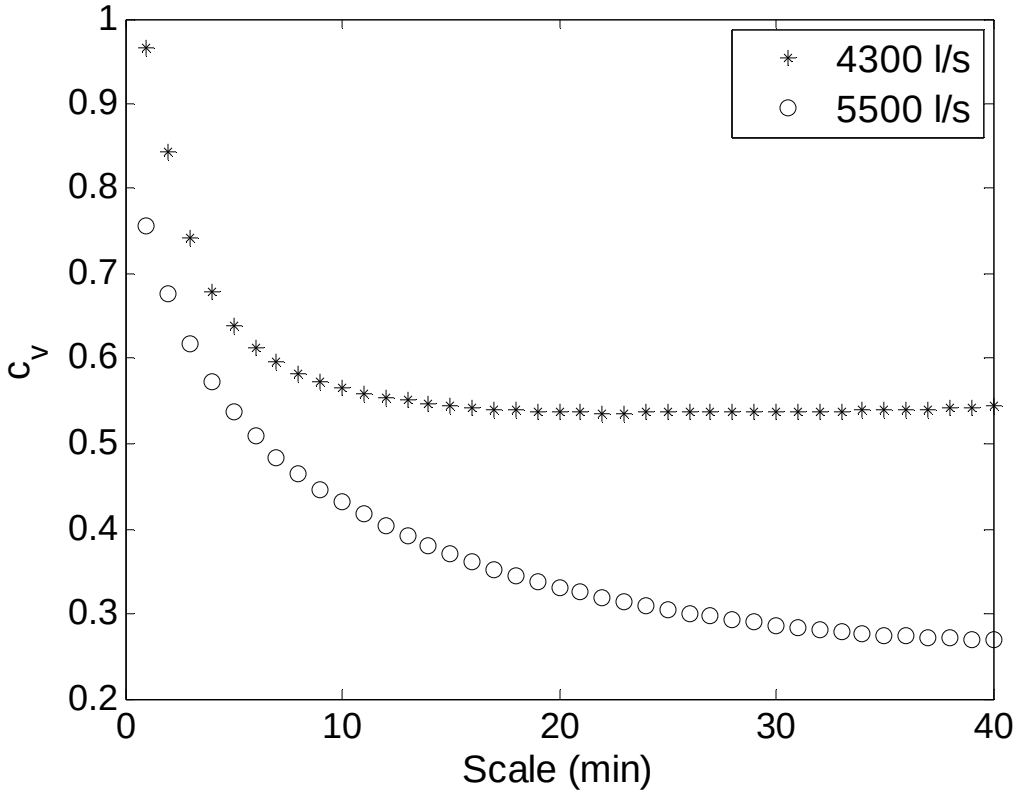

986

987 **Figure 7:** Coefficient of variation of the bedload sediment transport series.

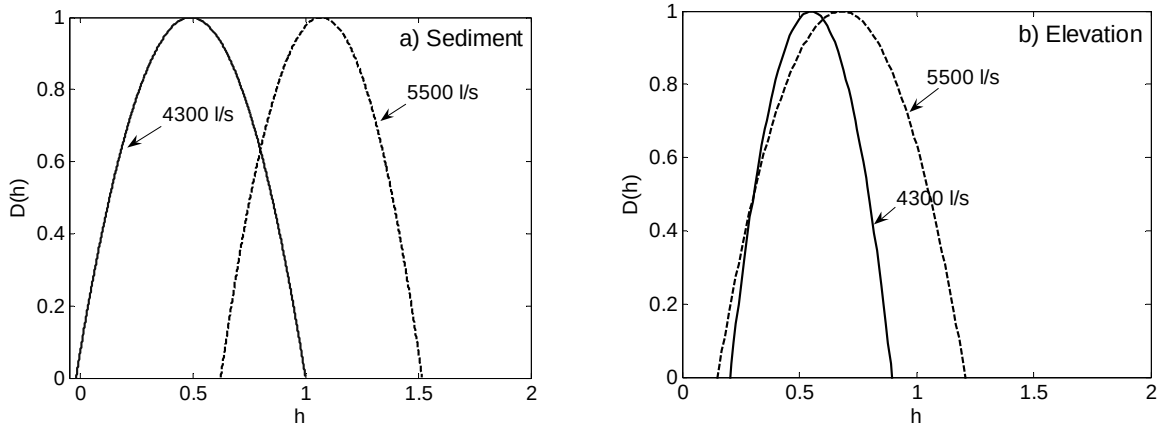

988
989

990 **Figure 8**: Fitted quadratic singularity spectra $D(h)$ obtained for (a) bedload sediment transport

991 series and (b) bed elevation fluctuation series respectively for the low and high discharge cases.

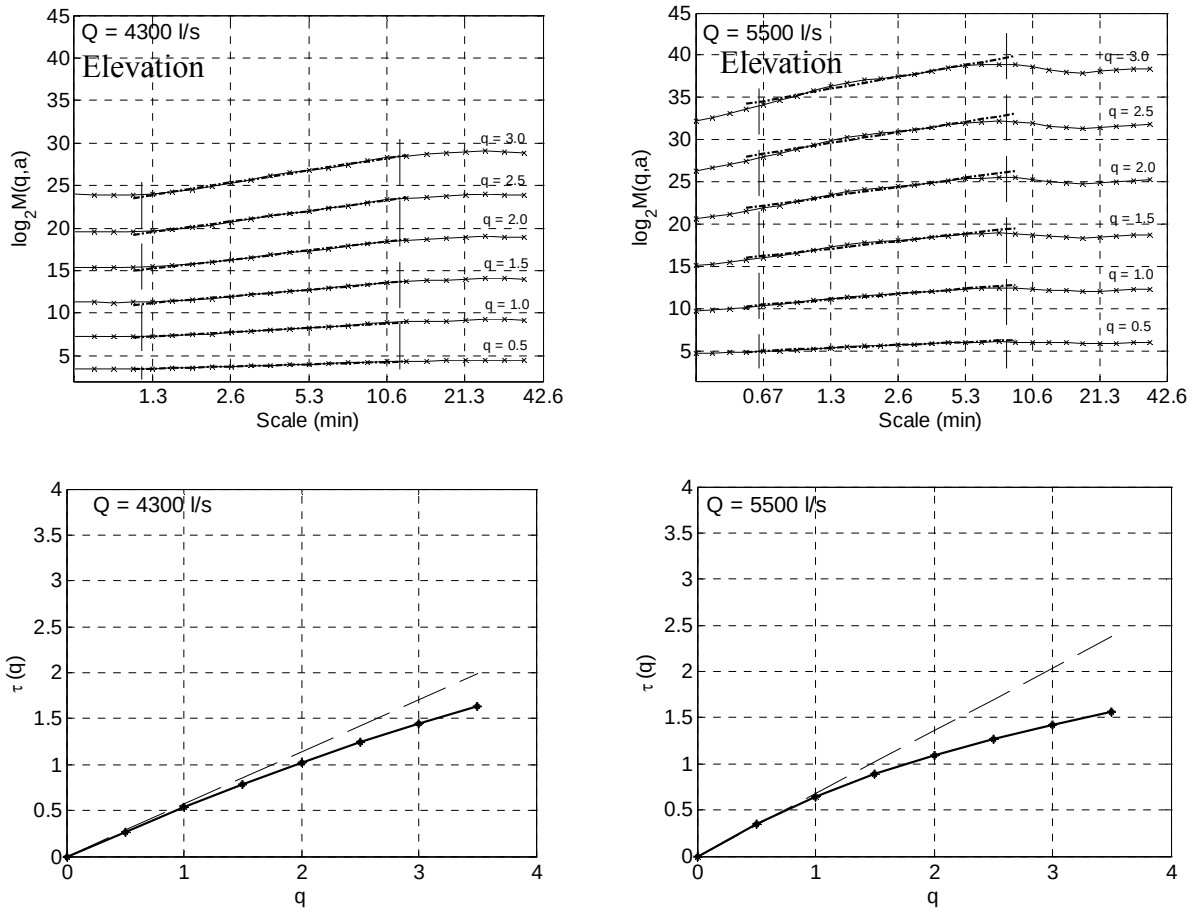

992

993

994

995 **Figure 9:** (top) Statistical moments of the fluctuations of the bed elevation time series as a

996 function of scale and (bottom) the scaling exponents $\tau(q)$ estimated from the log-log linear

997 regressions within the scaling regions. Notice the deviation of $\tau(q)$ from the linear line

998 establishing the presence of multifractality. (left) For low-transport conditions and (right) for

999 high-transport conditions.

1000

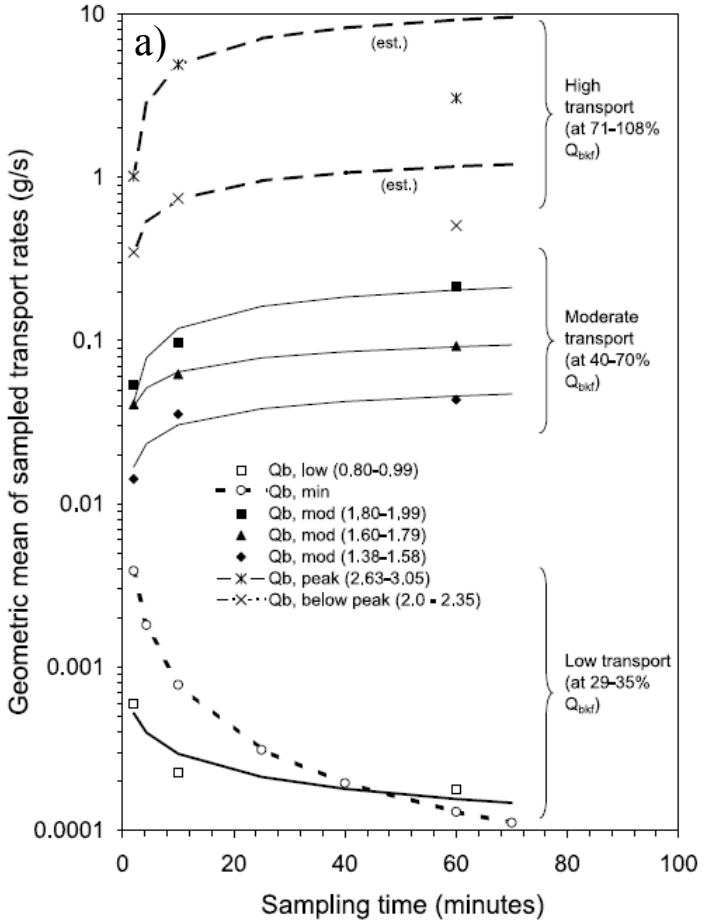
a)
(est.)
(est.)
High transport (at 71-108% Q_{bkf})
Moderate transport (at 40-70% Q_{bkf})
Low transport (at 29-35% Q_{bkf})
Qb, low (0.80-0.99)
Qb, min
Qb, mod (1,80-1,99)
Qb, mod (1.60-1.79)
Qb, mod (1.38-1.58)
Qb, peak (2.63-3.05)
Qb, below peak (2.0 - 2.35)
Geometric mean of sampled transport rates (g/s)
Sampling time (minutes)
10
1
0.1
0.01
0.001
0.0001
0
20
40
60
80
100

1001

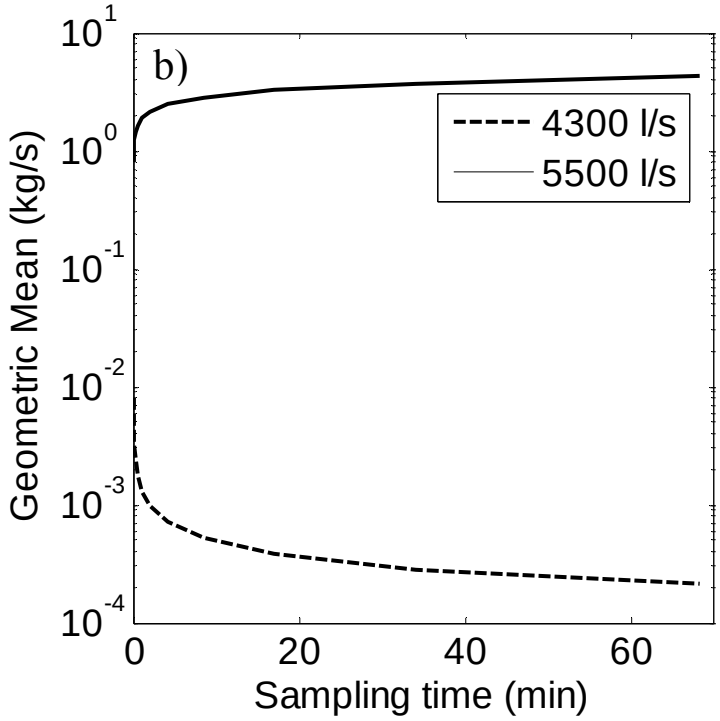
b)
4300 l/s
5500 l/s
Geometric Mean (kg/s)
Sampling time (min)
10^{1}
10^{0}
10^{-1}
10^{-2}
10^{-3}
10^{-4}
0
20
40
60

1002

Figure 10: Geometric means at different sampling times from: (a) field experiments [reproduced from *Bunte and Abt*, 2005], and (b) theoretical results from this study.

Appendix 1

Table A1: Multifractal parameters estimated for low and high flows using different Gaussian wavelets (see text for definitions)

Q (l/s)	Shields stress	Pan	Scaling Range (min)	Wavelet	c_1	c_2
4300	0.085	2	1.2-10	g2	0.57	0.12
		2	1.2-10	g3	0.56	0.14
		2	1.2-10	g4	0.54	0.12
		3	1.2-10	g2	0.52	0.11
		3	1.2-10	g3	0.49	0.13
		3	1.2-10	g4	0.48	0.13
		4	1-8	g2	0.49	0.10
		4	1-8	g3	0.47	0.10
		4	1-8	g4	0.45	0.10
5500	0.196	2	1-10	g2	1.04	0.09
		2	1-10	g3	1.07	0.09
		2	1-10	g4	1.09	0.10
		3	1-10	g2	1.04	0.11
		3	1-10	g3	1.07	0.10
		3	1-10	g4	1.09	0.11
		4	1-10	g2	1.09	0.11
		4	1-10	g3	1.12	0.11
		4	1-10	g4	1.14	0.11

b)